Highly Mismatched Crystalline and Amorphous GaN$_{1-x}$As$_x$ Alloys in the Whole Composition Range

K. M. Yu[1], S. V. Novikov[2], R. Broesler[1], I. N. Demchenko[3,4,5], J. D. Denlinger[3], Z. Liliental-Weber[1], F. Luckert[6], R. W. Martin[6], W. Walukiewicz[1], and C. T. Foxon[2]

[1]Materials Sciences Division, Lawrence Berkeley National Laboratory, 1 Cyclotron Road, Berkeley, CA 94720-8197, USA
[2]School of Physics and Astronomy, University of Nottingham, Nottingham NG7 2RD, UK
[3]Advanced Light Source, Lawrence Berkeley National Laboratory, 1 Cyclotron Road, Berkeley, CA 94720-8197, USA
[4]Department of Chemistry, University of Nevada Las Vegas, 4505 Maryland Pkwy-Box 454003, Las Vegas, NV 89154-4003, USA
[5]Institute of Physics PAS, al. Lotnikow 32/46, 02-668, Warsaw, Poland
[6]Department of Physics, SUPA, Strathclyde University, Glasgow, G4 0NG, UK

ABSTRACT

Alloying is a commonly accepted method to tailor properties of semiconductor materials for specific applications. Only a limited number of semiconductor alloys can be easily synthesized in the full composition range. Such alloys are, in general formed of component elements that are well matched in terms of ionicity, atom size and electronegativity. In contrast there is a broad class of potential semiconductor alloys formed of component materials with distinctly different properties. In most instances these mismatched alloys are immiscible under standard growth conditions. Here we report on the properties of $GaN_{1-x}As_x$ a highly mismatched, immiscible alloy system that was successfuly synthesized in the whole composition range using a non-equilibrium low temperature molecular beam epitaxy technique. The alloys are amorphous in the composition range of $0.17<x<0.75$ and crystalline outside this region. The amorphous films have smooth morphology, homogeneous composition and sharp, well defined optical absorption edges. The bandgap energy varies in a broad energy range from ~3.4 eV in GaN to~0.8 eV at x~0.85. The reduction of the band gap can be attributed primarily to the downward movement of the conduction band for alloys with x>0.2, and to the upward movement of the valence band for alloys with x<0.2. The unique features of the band structure offers an opportunity of using $GaN_{1-x}As_x$ alloys for various types of solar power conversion devices.

1. The Ga-N-As Alloy system

1.1 Dilute alloys

Semiconductor alloys formed through substitution of atoms with very different electronegativity and/or size have been known as highly mismatched alloys (HMAs). Because of large miscibility gaps, typically HMAs consist of a semiconductor matrix (elemental or compound) with the substitution of a small amount (up to several percents) of distinctly different isovalent atoms. The HMAs show large band gap reduction and their electronic structure is drastically different from their host materials. This is in contrast to conventional semiconductor alloys such as AlGaAs and GaAsP whose physical, electronic and optical properties can be deduced from a linear interpolation between their corresponding end point compounds with only a slight deviation, as predicted by the virtual crystal approximation (VCA). A most notable example of HMAs is the As-rich GaN_xAs_{1-x} in which strong band gap reduction by as much as 180 meV per mole percent of N has been observed [1,2,3,4]. The strong dependence of the band gap on the N content has made these diluted III-V nitrides important materials for a variety of applications, including long wavelength optoelectronic devices [5,6] and high efficiency hybrid solar cells [7,8].

In contrast to the very extensively studied As-rich GaNAs alloys much less work has been devoted to HMAs on the N-rich side of this alloy system. It was found that GaN doped with As at low, impurity like levels shows a characteristic blue emission at room temperature. At higher As doping levels an abrupt decrease in the band gap of resulting $GaN_{1-x}As_x$ alloys was observed [9,10,11,12]. Fig. 1 shows the experimental

band gap of both As-rich [2] and N-rich [12] GaNAs HMAs. It is obvious that these data

cannot be explained by a virtual crystal approximation (VCA) represented by the dashed

line. The dotted line in Fig. 1 shows a forced quadratic fitting to the experimental gap

energies on both sides with a single bowing parameter of b=16.2 eV. This bowing

parameter is in agreement with the value reported in Kimura et al. [11] According to this

fitting curve the bandgap would rapidly close up from both sides and become negative for

0.25<x<0.9.

1.2 Band anticrossing in highly mismatched III-V diute alloys

The unusually strong dependence of the fundamental gap on the N content in the

group III-N-V alloys has been the subject of many theoretical investigations [3,4].

Among these works, the band anticrossing model (BAC) [1,13,14] has been very

successful in explaining the experimentally observed electronic structures of the dilute

As-rich $GaN_{1-x}As_x$ alloys. The BAC model takes into account an anticrossing interaction

between localized N states and the extended states of the host semiconductor matrix.

Such interaction splits the conduction band into two subbands, E_- and E_+. The downward

shift of the lower subband (E_-) is responsible for the reduction of the fundamental band

gap and the optical transition from the valence band to the upper subband (E_+) accounts

for the high-energy edge. More recently, the BAC model has also been extended to

HMAs where a small fraction of metallic isovalent atoms substitute more electronegative

host atoms as occurs in the dilute N-rich $GaN_{1-x}As_x$ alloys where a small fraction of N

atoms is substitued by As. In this case due to the substantial difference in the ionization

energies of the As and N anions, the p-states of the substitutional As atoms form resonant

levels above the valence band edge of GaN. The As derived localized states interact strongly with the extended p-states of the host. The interaction splits the valence band into a series of E_+ and E_- sub-bands with dispersion relations that are dependent on the As concentration [12,14]. This valence band anticrossing (VBAC) has been successful in explaining the valence band restructuring in many dilute alloys where a small fraction of the anions are replaced by more metallic impurities, including $GaBi_xAs_{1-x}$ [15,16], $GaSb_xAs_{1-x}$ [17] and Sn_xGe_{1-x} [18].

Wu et al. [12] investigated the BAC in N-rich and As-rich GaNAs alloys with a limited range of composition and interpolated the composition dependence of the band gap of $GaN_{1-x}As_x$ alloys over the entire composition shown by the solid curve in Fig. 1. The calculations predict a minimum band gap of 0.7 eV at $x{\sim}0.8$. This is in a stark contrast to the composition dependence of the band gap predicted by the VCA and the quadratic fitting with b=16.2 eV. However, neither of these predictions could be tested as there has been no experimental data for alloys in the middle 85% of the alloy composition.

2. Low Temperature Molecular Beam Epitaxial Growth of Ga-N-As

During the last 15 years there has been considerable theoretical and experimental interest in As-doped GaN. However, due to the large miscibility gap for the Ga-N-As system, alloys with large compositions have not been achieved. $GaN_{1-x}As_x$ alloys at the N-rich end of the phase diagram have been grown by metal-organic vapour phase epitaxy (MOVPE) and by molecular beam epitaxy (MBE) [9]. For both techniques, it is difficult to obtain a high concentration of As in the alloy before phase separation occurs. The

highest reported As content in MOVPE grown layers is $x \sim 0.067$ [10,11,12]. Even lower maximum As contents of $x \sim 0.0026$ [19] and $x \sim 0.01$ [20] were achieved in MBE layers grown at $.750^oC$ and at 500^oC, respectively

Recently, materials with constituents having drastically different chemical or physical properties at compositions or structures far exceeding their thermodynamic solubility and stability limits have been synthesized using extreme non-equilibrium synthesis techniques [21,22,23]. The atomic diffusion length in these non-equilibrium processes is long enough to form crystalline lattices with uniform compositions, but short enough to avoid equilibrium phase segregation. This has been recently demonstrated in the growth of single phase ferromagnetic $Ga_{1-x}Mn_xAs$ with Mn concentration as high as 16% using the low temperature MBE technique (LT-MBE) [23,24]. It is known that in MBE the As solubility limit in $GaN_{1-x}As_x$ alloys is increasing with decreasing growth temperature [20,25]. In this study LT-MBE has been employed to overcome the miscibility gap in the $GaN_{1-x}As_x$ alloy system, allowing the synthesis of thin films of $GaN_{1-x}As_x$ alloys over the whole composition range.

All GaNAs samples were grown on 2 inch sapphire (0001) substrates by plasma-assisted MBE in a MOD-GENII system. The system has a HD-25 Oxford Applied Research RF activated plasma source to provide active nitrogen and elemental Ga is used as the group III-source. In all experiments we have used arsenic in the form of As_2 produced by the Veeco arsenic valved cracker. The MBE system is equipped with reflection high energy electron diffraction (RHEED) facility (12kV) for surface reconstruction analysis. For the growth of all GaNAs samples, we have used the same active N flux with the total N beam

equivalent pressure (BEP) ~1.5 10^{-5} Torr and the same deposition time (2hr) for the majority of the films.

The composition of the films was measured by Rutherford backscattering spectrometry (RBS) and particle induced x-ray emission (PIXE) using a 2 MeV He ion beam and further confirmed by wavelength-dispersive x-ray (WDX) spectroscopy using a 5 keV electron beam. Compositon mapping by WDX with ~1 μm resolution found no discernable compositional variation over a 256x256 μm region in the films. Fig. 2 shows the As composition in $GaN_{1-x}As_x$ films grown by LT- MBE measured by RBS/PIXE as a function of growth temperature, the dashed line in the figure is a quadratic fit of the data. The Ga and As_2 flux in these growths were kept constant with BEP ~$1.5x10^{-7}$ and ~$7.5x10^{-6}$ Torr, respectively. A monotonic increase in the As incorporation in the film is observed as the growth temperature is reduced. We note that as the growth temperature decreases, along with the increase in As content in the film, the film loses its crystallinity and becomes amorphous (close circle symbols in Fig. 2).

3. Structure of LT-MBE $GaN_{1-x}As_x$

We found that epitaxy of $GaN_{1-x}As_x$ under Ga-rich growth conditions at relatively high temperatures of ~600^oC results in phase sepatation into GaN:As and GaAs:N for x>0.02. This is evident from the the appearance of GaAs (111) diffraction peak in the x-ray diffraction (XRD) pattern shown in Fig. 3 (b). The overall GaAs mole fraction x determined by RBS and PIXE for this film is x~0.1. However, XRD result in Fig. 3 (b) showed that instead of a random alloy of $GaN_{0.9}As_{0.1}$, phase separation occurs in this film

and two phases coexist in the film: ~10% GaAs:N and ~90% GaN:As. Note that high quality GaN epitaxial films were grown by MBE on sapphire typically at ~800°C. As the growth temperature is reduced from ~600 to 100°C, along with the increase in the As incorporation from x~0.02 to 0.7, the structure of the $GaN_{1-x}As_x$ film transforms from single crystalline to polycrystalline (~500°C) to amorphous (<410°C). Fig. 3(a) shows a series of XRD patterns from $GaN_{1-x}As_x$ films grown with the same As and Ga fluxes, but at different growth temperatures. The shift of the GaN 0002 diffraction peak to lower diffraction angle for the crystalline $GaN_{1-x}As_x$ films (with x<0.17) is consistent with the increase in lattice parameter due to the incorporation of As into the N sublattice (bond length R_{Ga-N}~0.195 nm and R_{Ga-As}~0.246 nm). The absence of any diffraction peak from films with x>0.17 grown at temperature <400°C suggests that these films are amorphous. However, the presence of small fraction of nanocrystalline materials that is beyond the sensitivity of the XRD technique cannot be ruled out.

It is worth noting that even as the growth temperature is reduced to 200°C, GaN films grown without As flux are still crystalline. Transmission electron microscopy (TEM) study shows that such GaN films are still epitaxial with high density of dislocations and small columns (30-50 nm). Amorphous GaN (a-GaN) has been proposed to be an electronic material with technological potential since theoretical study predicted no deep gap states and therefore no deep carrier traps in this material [26]. These desirable properties are a consequence of the lack of homopolar bonds in a-GaN because of its high ionicity. Despite many attempts on the synthesis of a-GaN using a variety of methods, stoichiometric, single phase GaN thin films with unambiguous amorphous signature have not been achieved so far [27,28,29]. This is believed to be due to the high ionicity of GaN. In fact, ion implantation

studies revealed that dynamic annealing is very strong in GaN. Amorphization of GaN under very heavy ion irradiation (Au) even at 77 K appeared to be similar to that in Si or GaAs at elevated implant temperature [30]. This is qualitatively similar to our finding that highly defective single crystalline GaN is formed by LT-MBE growth even at 200°C (~600°C below the normal MBE growth temperature). When significant amount of As (>17%) is incorporated into the lattice of GaNAs in our studies, ionicity of the crystal is reduced and the film becomes amorphous.

As the alloy composition is pushed to the As-rich side of $GaN_{1-x}As_x$ alloys by increasing the Ga flux from a BEP~$1.5x10^{-7}$ Torr to ~$6x10^{-7}$ Torr at the growth temperatures of ~200°C, the film structure changes from amorphous to crystalline again. Fig. 3 (b) shows a series of As-rich $GaN_{1-x}As_x$ films with x=0.62 to 0.86 grown at ~200°C with increasing Ga flux. XRD pattern from the phase separated $GaN_{0.9}As_{0.1}$ film grown at 600°C under Ga-rich conditions showing both the cubic GaAs (111) and wurtzite GaN (0002) peaks is also shown in Fig. 3(b) for comparison.

As the arsenic content in the $GaN_{1-x}As_x$ film increases to higher than 75%, the films becomes crystalline with primarily polycrystalline As-rich cubic $GaN_{1-x}As_x$ with small amount of wurtzite N-rich $GaN_{1-x}As_x$. The incorproation of N in the As sublattice is evident from the shift of the cubic $GaN_{1-x}As_x$ (111) peak to higher diffraction angle as compared to GaAs (111) peak indicating a decrease in the lattice parameter. A $GaN_{1-x}As_x$ film with x~0.86 shows a single cubic phase with strong and narrow (111) diffraction peak suggesting that the film is polycrystalline with larger grain size as the alloy becomes more As-rich.

The microstructure of the $GaN_{1-x}As_x$ films was investigated using cross sectional transmission electron microscopy. A JEOL 3010 with 300 keV accelerating energy and a

resolution of 2.4Å, JEOL CM300 with sub-Angstrom resolution and a Philips Tecnai microscope for Z-contrast high resolution studies were used. Fig. 4 (a) shows a series of selective area electron diffraction pattern (SAD) from alloys with increasing As content as a result of decreasing growth temperature from 550 to 100°C. The SAD results unambiguously illustrate that the $GaN_{1-x}As_x$ alloys go from single crystalline spot pattern (T_g=550°C) to polycrystalline ring pattern (400°C<T_g<500°C) to amorphous diffuse ring pattern (T_g<400°C; x>0.2). The diffuse ring patterns for $GaN_{1-x}As_x$ alloys with x in the range of ~0.2 to 0.75 confirm that these alloys are amorphous with no observable nanoscale secondary phases. We also found that at the same growth temperature, the As content in the amorphous film increases with the As flux during growth. This is illustrated in Fig. 4(a) with the SAD patterns from two amorphous samples grown at 210°C: the sample with 45% As was grown with ~6X higher As flux as the sample with 27% As. The SAD pattern for the As-rich $GaN_{1-x}As_x$ film with x= 0.86 grown at ~200°C is also shown in Fig. 4 (a). The ring pattern for this sample is consistent with the XRD result (Fig. 3 (b)) that cubic polycrystalline phase of $GaN_{1-x}As_x$ was formed for As-rich alloys.

Fig. 4(b) shows two typical cross-sectional TEM micrographs of a crystalline $GaN_{1-x}As_x$ (x=0.02; T_g=550°C) and an amorphous film (x=0.45; T_g=210°C). TEM micrograph of the 2% As film reveals a columnar crystalline film with high density of planar defects. These columns are misoriented with respect to each other; therefore dislocations need to form to accommodate this misorientation. The inset in the figure shows a high resolution micrograph of this film showing the presence of stacking faults in the film. The micrograph of the high As content $GaN_{1-x}As_x$ layer (45% As) shows that

the film is uniform and smooth. The high resolution micrograph shown in the inset further confirms the amorphous nature of this film with no observable composition segregation.

4. Band gap and electronic structures of GaN$_{1-x}$As$_x$ over the entire composition

The optical gap of the GaN$_{1-x}$As$_x$ alloys were measured by absorption using a LAMBDA-950 UV/Vis/NIR spectrophotometer over the range of 190-3300 nm. Fig. 5 plots the square of the absorption coefficient (α^2) as a function of energy for a series of crystalline and amorphous GaN$_{1-x}$As$_x$ films over the entire composition range. Notice that the films in the composition range of 0.17<x<0.75 are amorphous while those outside this range are crystalline (either single crystallibe or polycrystalline). Samples that are phase separated are not included here. The band gap of the GaN$_{1-x}$As$_x$ alloys can be estimated by extrapolating the linear part of the α^2 down to the energy axis (dash lines shown in the figure). A strikingly sharp band gap absorption is observed in all films. This is particularly significant for the amorphous films since this suggests that the density of gap states in the amorphous films are low, consistent with the predicted low number of homopolar bonds in nitride based alloys [26]. Some small features below the band gap can be attributed to the Fabry-Perot oscillations indicating uniform film thickness with a smooth surface and of the films with sharp film-substrate interface. We note that while the crystalline and amorphous GaN$_{1-x}$As$_x$ alloys may be materials with very different properties, similar to crystalline and amorphous silicon, it is interesting to compare these properties directly, especially when very little is known about amorphous nitride

materials [26]. Despite the crystalline and amorphous transition the absorption results in

Fig. 5 show a continuously montonic decrease in the band gap as the As content

increases. This provides additional support to the claim that the films are single phase

with no phase separation in the crystalline state, and no composition non-uniformity in

the amorphous state.

Fig. 6 summarizes the composition dependence of the optical band gap energy for

both crystalline (open symbols) and amorphous (solid symbols) $GaN_{1-x}As_x$ alloys. These

experimental data are compared directly with calculated composition dependence of the

band gap as shown in Fig. 1. It is obvious from Fig. 6 that the band gap values for the

$GaN_{1-x}As_x$ alloys cannot be explained by the VCA or the fitted curve using a single

bowing parameter of 16.2 eV. Excellent agreement can be observed between the band

gap values for the crystalline alloys and the BAC model. The deviation of the

experimental results from the BAC calculations found for the amorphous alloys is not

unexpected as the model has been developed for crystalline materials. Additional

uncertainty is introduced by the fact that the band gap has been calculated as a

composition weighted interpolation of the BAC model results and is less accurate for the

alloys in the middle range of compositions.

According to the BAC model the observed reduction of the band gap can be

attributed to an upward shift of the valence band edge and a downward movement for the

conduction band edge in the N-rich and As-rich dilute $GaN_{1-x}As_x$ alloys, respectively.

However, the absolute movement of the conduction and valence bands of the $GaN_{1-x}As_x$

alloys cannot be derived from our optical measurements. To directly measure the band

positions we used the combination of soft x-ray emission (SXE) and absorption (XAS)

spectroscopies. XAS and SXE directly probe the partial density of states (DOS) of the conduction band and valence band, respectively [31]. Overlapping the SXE and XAS spectra with reference to the core level provides a direct measurement of the energy positions of the valence and conduction band states in semiconductor materials. In this work, the Nitrogen K-edge (around 400 eV) was investigated at room temperature at the Advanced Light Source (ALS) on beam line 8.0.1. XAS was detected by the total fluorescence yield detection mode with an energy resolution of about 0.2 eV, and SXE was measured using the Tennessee/Tulane grating spectrometer with a total energy resolution of 0.6 eV.

Figure 7 shows the SXE and XAS spectra for a number of selected $GaN_{1-x}As_x$ samples excited at the nitrogen K-edge. During normalization of XAS spectra a pre-edge linear background was subtracted and the edge step was normalized to unity (at 440 eV). The elastic emission peak in SXE spectra was used for calibration of the detector energy to the XAS monochromator energy. The inset in Fig. 7 presents the zoom-in region showing the valence band edge (VBE) and conduction band edge (CBE). The XAS threshold energy defines the CBE with respect to the N 1s core-level. The threshold absorption profiles are shown as the right-hand part of the curves in Fig. 7. The excitation energy was then tuned to the onset of the conduction band and the resultant SXE due to electronic transitions from the upper valence band to the N K-shell was recorded with a wavelength-dispersive detector. The SXE spectra are shown in Fig. 7 on the left-hand side. In this way the absolute positions of the conduction band and valence band edges are directly measured as a function of composition and compared to the results of conventional optical measurements.

The most striking changes in the spectra in Fig. 7 are the rapid broadening and suppression of sharp features of the XAS profiles with increasing As content. First the three prominent peaks in pure GaN are significantly reduced in amplitude and slightly broadened for alloys with a very dilute amount of As (x=0.02). This behavior is consistent with a small amount of structural disorder and a loss of orientational order of polycrystalline grains of the anisotropic wurtzite structure of GaN. This is confirmed with polarization dependent XAS spectra of these samples (not shown). With increasing As-content, the XAS spectra are transformed into very featureless smooth profiles for x=0.17-0.70 consistent with the complete loss of long-range periodicity in the amorphous state.

Furthermore, very different XAS threshold lineshapes are observed for crystalline and amorphous alloys as shown in the inset of Fig. 7. For GaN and dilute As polycrystalline films, we observe a very gradual onset (at 398.2 eV) that arises from a single isolated band with light effective mass that disperses down from the main CB DOS and exhibits a quadratic-like DOS profile that is related its non-parabolic dispersion. The amorphous XAS threshold profiles, on the other hand, exhibit an abrupt ~1 eV shift to lower threshold energy but with profile very amenable to linear extrapolation. The increasing slope of this linear onset from x=0.17 to x=0.45 and then relatively constant for alloys with x up to ~0.70 can be understood as a gradually increasing amount of hybridization of N 2p partial density with As conduction states. The strength of this N hybridization with near neighbor As atoms reaches a maximum at 50% As stoichiometry.

Despite the large changes in the XAS profile for dilute As (x=0.02), the threshold energy and gradual onset profile was unchanged. Hence the CBE is not responsible for

the large ~0.8 eV decrease in the optical band gap observed for dilute As content [12]. Instead, observable in the SXE threshold region of Fig. 7 inset is a weak high energy foot that develops at the VBE. The VB change is consistent with valence N states hybridizing with an As impurity level just above the GaN valence band maximum which is the basis for the BAC model of the band gap reduction in this dilute doping regime [12]. For increasing As-content into the amorphous phase, the threshold energy of the this VBE foot increases only a small amount while the intensity grows steadily due the increasing amount of near neighbor As atoms which hybridize with the N-p states.

Finally for the As-rich region represented in Fig. 7 by the sample with x=0.86, both the SXE and XAS profiles exhibit dramatic changes. The SXE spectrum of this cubic GaAs-like polycrystalline phase develops again a sharp two-peak DOS profile but with a lineshape and peak maximum distinctly different from the polycrystalline phase of the hexagonal GaN-like dilute As region. The XAS profiles for the alloy with x=0.86 also exhibits a dramatic new sharp peak just above threshold. Rather than indicative of a structural change, this sharp peak reflects the existence of a localized N impurity level above the GaAs conduction band minimum. The development of this localized state into a narrow band via hybridization with GaAs conduction states is the source of the rapid band gap reduction from pure GaAs within the BAC model [1,14].

The composition dependence of the CBE and the VBE energies for $GaN_{1-x}As_x$ alloys as measured by XAS and SXE, including samples not displayed in Fig. 7, is shown in Fig. 8 together with the BAC predicted values. Again, we point out here that the calculated band movements by an interpolation of the BAC model are included for comparison purpose only. Band movements in the amorphous alloys may vary

dramatically from crystalline alloys. Both CBE and VBE are observed to shift as x increases. A rapid jump in the VBE to higher energy for dilute As (x<0.10) polycrystalline samples as compared to GaN is observed consistent with the BAC model. A second jump to lower energy is observed in the CBE upon entering into the amorphous phase (x>0.17). For increasing x in the amorphous phase, both the VBE and CBE are only very weakly shifting to higher and lower energies, respectively. Finally a smaller jump in the VBE yet again to a higher energy is observed for the amorphous to As-rich polycrystalline transition (x>0.70). Not unexpectedly the smooth interpolation of the BAC model from the dilute polycrystalline regions does not explain the discontinuous energy jumps into the amorphous phase. We also point out that the band gap energies measured by XAS and SXE are lower than the values obtained by optical absorption. This may be attributed to excitonic coupling between the screened core hole and conduction electron [32].

5. **Potential for photovoltaic applications**

The direct conversion of sunlight into hydrogen by photoelectrochemical (PEC) water-splitting is one of the simplest methods to convert solar energy into a storable fuel. The practical realization of this technology depends critically on the availability of a suitable electrode material that combines acceptable solar response and efficiency and sufficient service lifetime for energy payback. For efficient hydrogen production by PEC water splitting, an ideal photoelectrode must meet three criteria: corrosion stability, a band gap between 1.8 and 2 eV to produce sufficient over-potential to drive the water-

splitting reactions while still absorbing a significant fraction of the solar spectrum, and band edges straddling the hydrogen and oxygen redox potentials for spontaneous water splitting [33]. To date, no known material satisfies all these requirements. Several oxides, most notably TiO_2, have shown good corrosion stability under operation, but have low efficiencies due to their wide band gaps [33,34,35]. III-V and II-VI semiconductors, such as $GaInP_2$ [36], have shown high water-splitting efficiencies but these materials have poor corrosion resistance and showed performance degradation and/or short lifetimes.

For N-rich $GaN_{1-x}As_x$ alloys, as a result of the VBAC the band gap of GaN is effectively reduced by the rapid upward movement of the valence band edge while the conduction band moves down at a much slower rate. Furthermore it is known that GaN is a mechanically hard and corrosion resistant semiconductor. The N-rich $GaN_{1-x}As_x$ alloys with this unique electronic structure can be promising materials for the photoanodes for the direct conversion of sunlight into hydrogen by photoelectrochemical (PEC) water-splitting. The H_2/O_2 redox potentials (dotted lines) are shown in Fig. 8 together with composition dependence of the CB and VB positions of the $GaN_{1-x}As_x$. Within our experimental error, Fig. 8 shows that a $GaN_{1-x}As_x$ alloy with x~0.1 has a band gap of ~2.4 eV still straddling the hydrogen and oxygen redox potentials and thus is a promising material for high efficiency PEC water-splitting.

In addition to the PEC application, the $GaN_{1-x}As_x$ material system has many unique features in the electronic band structure that make it a good candidate for photovolatic applications. For example, this alloy system has a wide band gap tuneability covering a spectral range of ~0.8 to 3.4 eV. This spectral range provides an almost perfect fit to the solar spectrum offering the opportunity to design high efficiency

multijunction solar cells [37,38] using a single ternary alloy system. Since the absorption coefficient for the crystalline and amorphous $GaN_{1-x}As_x$ alloys is large, only thin films of about a micron are needed for this application. This makes the fabrication of multijunction cells simple and cost effective. The amorphous nature of this alloy over a wide alloy range (0.2<x<0.8) can also be advantageous since they can be deposited on low-cost glass substrate, further reducing the cost of such device. A simple 2-junction cell with a ~1.6 eV top subcell on a ~0.8 eV bottom cell can yield a maximum theoretical efficiency ~55% under maximum concenrtation [39] or ~42% under 1.5 AMO irradiation. This can be achieved using $GaN_{1-x}As_x$ alloys with x=0.8 and 0.4 as bottom and top subcells, respectively.

One major issue in the successful utilization of these alloys for PEC and PV devices is its transport properties. Investigation on both n and p-type doping of crystalline and amorphous $GaAs_xN_{1-x}$ alloys by growth and implantation techniques are underway.

5. Conclusion

We have successfully synthesized $GaN_{1-x}As_x$ alloys in the whole composition range using low temperature molecular beam epitaxy. Alloys in the composition range of 0.17<x<0.75 are amorphous. High resolution electron microscopy and electron diffraction studies clearly show that the amorphous films with high As contents are amorphous with no indication of composition non-uniformity. Optical absorption measurements show sharp absorption edges with a gradual decrease of the bandgap from ~3.4 eV to < 1 eV with increasing As content. The energy gap reaches its minimum of ~0.8 eV at x~0.8. The composition dependence of the band gap of the crystalline GaN_{1-}

$_x$As$_x$ alloys (x<0.2 and x>0.8) follows the prediction of the band anticrossing model well while the amorphous alloys show higher band gaps than predicted (by as much as ~0.6 eV). The reduction of the band gap can be attributed primarily to the downward movement of the conduction band minimum for alloys with x>0.2, and to the upward movement of the valence band maximum for alloys with x<0.2. The unusual electronic structure and capability for controlling the locations of the conduction and valence band edges offer unprecedented opportunity for using these alloys for novel solar power conversion devices.

FIGURE CAPTIONS

Figure 1. Energy gap E_g of dilute As-rich (ref. 2) and N-rich (ref 12) $GaN_{1-x}As_x$ alloys as a function of x reported in the literature. The solid line is the calculated band gap of dilute $GaN_{1-x}As_x$ alloys based on the band anticrossing model interpolated over the entire composition range. Band gaps by virtual crystal approximation (VCA) and by a forced quadratic fitting to the experimental gap energies using a single bowing parameter of *b*=16.2 eV are also shown.

Fig. 2 The Arsenic composition in $GaN_{1-x}As_x$ films grown by LT- MBE measured by RBS/PIXE as a function of growth temperature. The Ga and As_2 fluxes with BEP ~$1.5x10^{-7}$ and ~$7.5x10^{-6}$ Torr, respectively were used in these MBE growths.

Fig. 3 X-ray diffraction patterns from $GaN_{1-x}As_x$ films (a) in the N-rich regime grown at temperature from 200 to 550°C, and (b) in the As-rich regime grown at 200°C with increasing Ga flux. XRD pattern from a phase separated film grown at 600°C is also shown in (b) for comparison. The patterns are shifted vertically.

Fig. 4 (a) A series of selective area electron diffraction patterns (SAD) from $GaN_{1-x}As_x$ alloys with increasing As content as a result of decreasing growth temperature from 550 to 100°C. (b) Two typical cross-sectional TEM micrographs of a crystalline $GaN_{1-x}As_x$ (x=0.02; T_g=550°C) and an amorphous $GaN_{1-x}As_x$ film (x=0.45; $T_{g=}$210°C).

Fig. 5. The energy dependence of the square of the absorption coefficient α^2 for $GaN_{1-x}As_x$ layers grown at different temperatures from ~100^oC to ~600^oC.

Fig. 6 Dependence of the optical band gap energy on the value of x for crystalline and amorphous $GaN_{1-x}As_x$ alloys. Calculated composition dependence of the band gap of $GaN_{1-x}As_x$ alloys based on the band anticrossing model (BAC), virtual crystal approximation (VCA) and using a single bowing parameter extracted from dilute alloys (b=16.2 eV) are also shown.

Fig. 7 Fig. 7 The nitrogen *K*-edge SXE and total fluorescence yield XAS of $GaN_{1-x}As_x$ films with different As fractions. An elastic emission peak in the threshold-excited SXE is used for energy calibration to XAS. The inset shows the magnified view of the XAS and SXE threshold regions.

Fig. 8 Composition dependence of the conduction band minimum (CBM) and the valence band maximum (VBM) energies for $GaN_{1-x}As_x$ alloys as measured by XAS and SXE, respectively plotted together with the BAC predicted values. The linear interpolations of CB and VB between end point compounds (GaN and GaAs) are also shown. Positions of the the H_2/O_2 redox potentials with respect to the VB maximum of GaN are also shown.
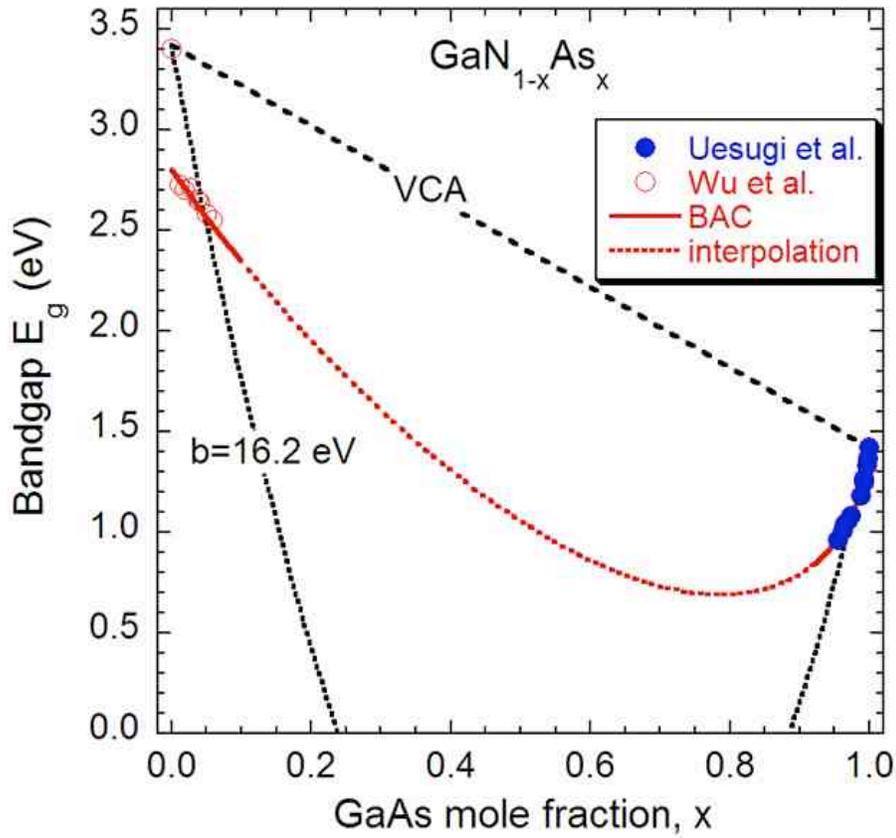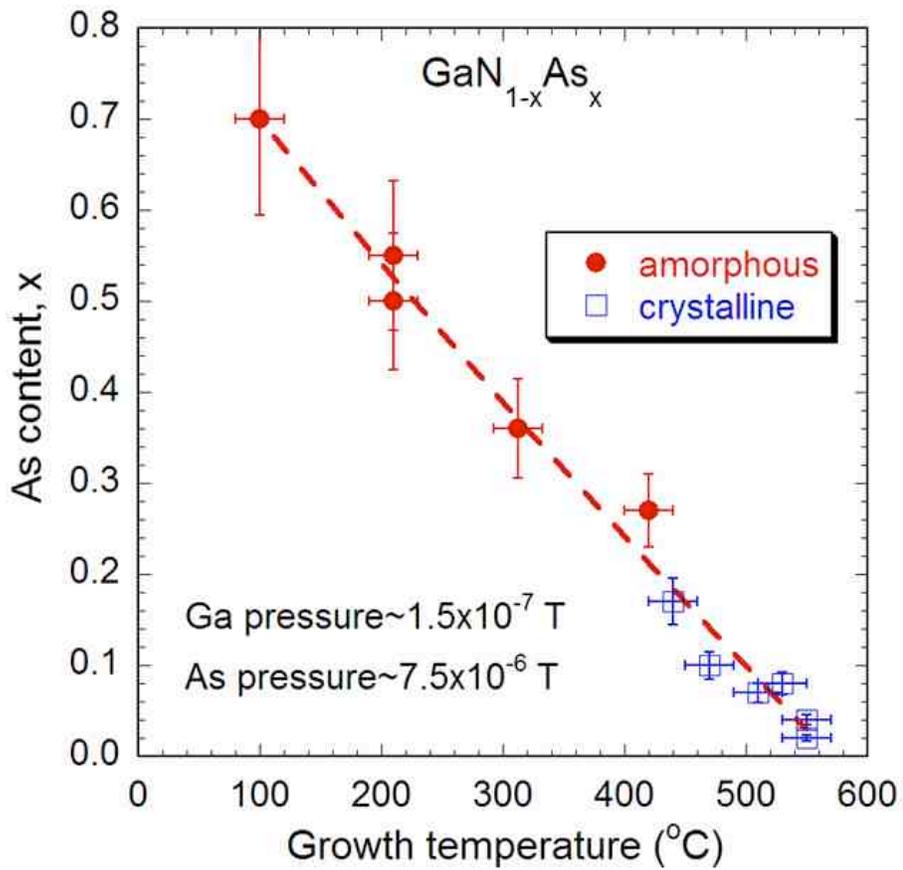
Figure 1

Figure 1. Energy gap E_g of dilute As-rich (ref. 2) and N-rich (ref 12) $GaN_{1-x}As_x$ alloys as a function of x reported in the literature. The solid line is the calculated band gap of dilute $GaN_{1-x}As_x$ alloys based on the band anticrossing model interpolated over the entire composition range. Band gaps by virtual crystal approximation (VCA) and by a forced quadratic fitting to the experimental gap energies using a single bowing parameter of b=16.2 eV are also shown.

Figure 2

Fig. 2 The Arsenic composition in $GaN_{1-x}As_x$ films grown by LT- MBE measured by RBS/PIXE as a function of growth temperature. The Ga and As_2 fluxes with BEP ~1.5x10^{-7} and ~7.5x10^{-6} Torr, respectively were used in these MBE growths.
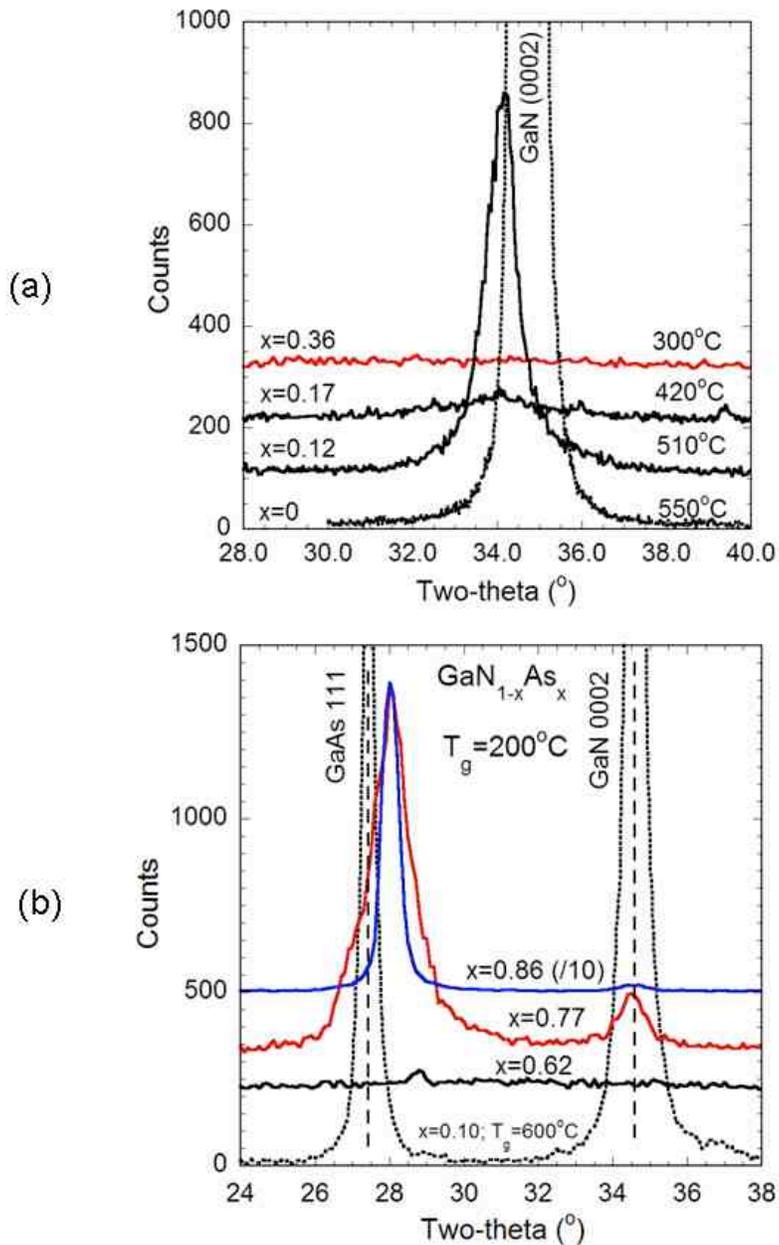
Figure 3

Fig. 3 X-ray diffraction patterns from $GaN_{1-x}As_x$ films (a) in the N-rich regime grown at temperature from 200 to 550°C, and (b) in the As-rich regime grown at 200°C with increasing Ga flux. XRD pattern from a phase separated film grown at 600°C is also shown in (b) for comparison. The patterns are shifted vertically.
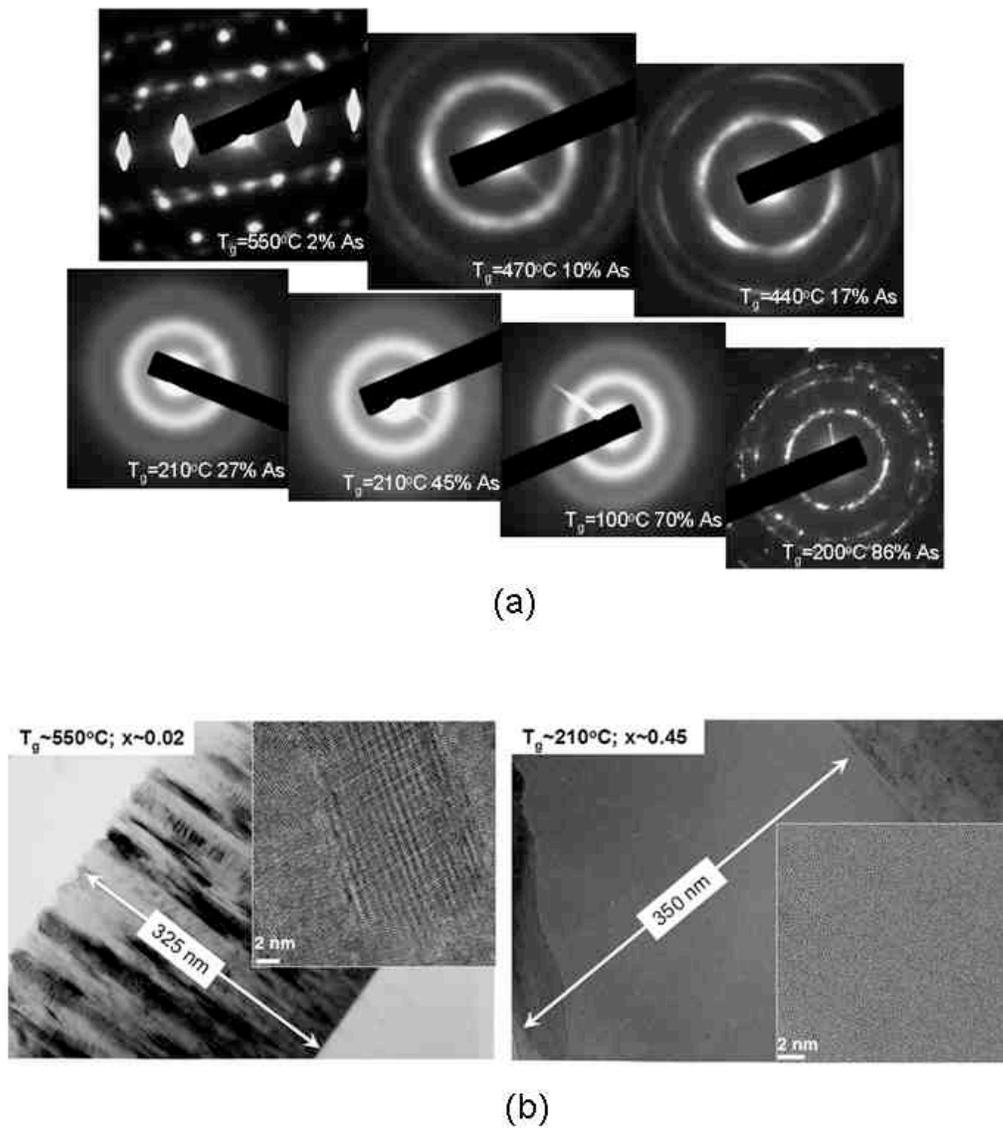
(a)

(b)

Figure 4

Fig. 4 (a) A series of selective area electron diffraction patterns (SAD) from $GaN_{1-x}As_x$ alloys with increasing As content as a result of decreasing growth temperature from 550 to 100°C. (b) Two typical cross-sectional TEM micrographs of a crystalline $GaN_{1-x}As_x$ (x=0.02; T_g=550°C) and an amorphous $GaN_{1-x}As_x$ film (x=0.45; T_g=210°C).
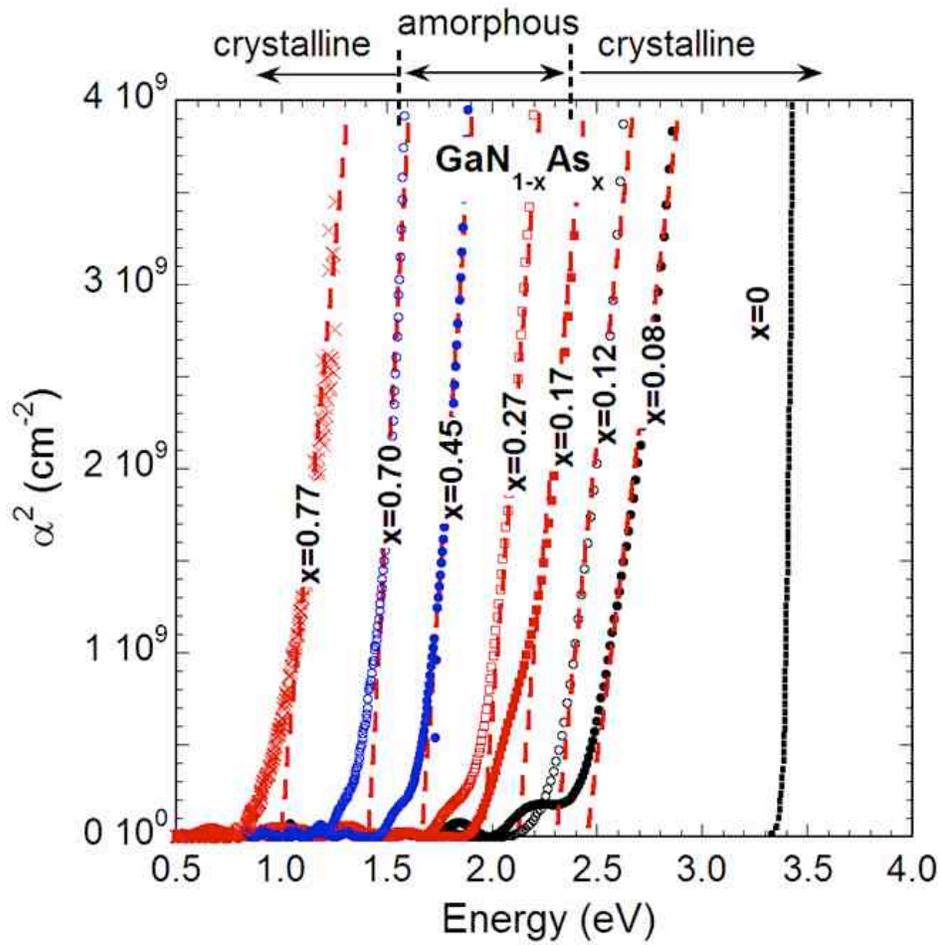
Fig. 5. The energy dependence of the square of the absorption coefficient α^2 for $GaN_{1-x}As_x$ layers grown at different temperatures from $\sim 100^o$C to $\sim 600^o$C.
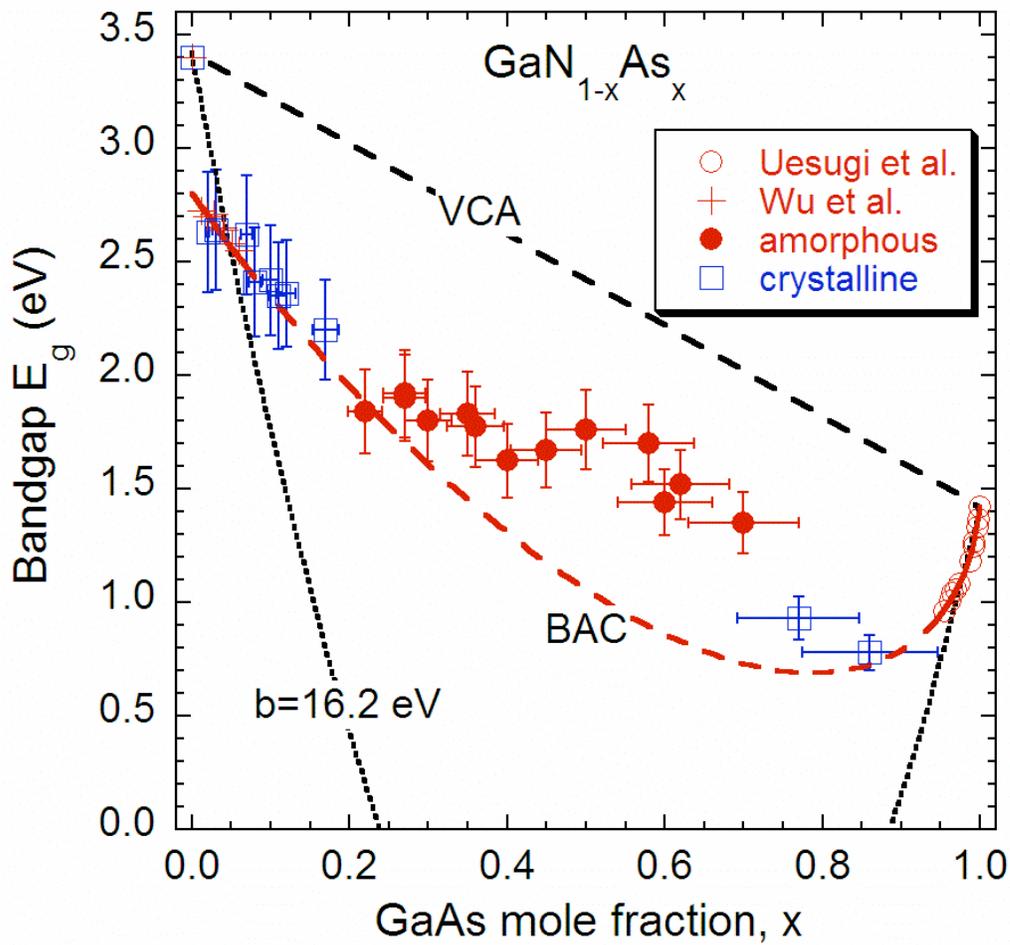
Fig. 6 Dependence of the optical band gap energy on the value of x for crystalline and amorphous $GaN_{1-x}As_x$ alloys. Calculated composition dependence of the band gap of $GaN_{1-x}As_x$ alloys based on the band anticrossing model (BAC), virtual crystal approximation (VCA) and using a single bowing parameter extracted from dilute alloys (b=16.2 eV) are also shown.
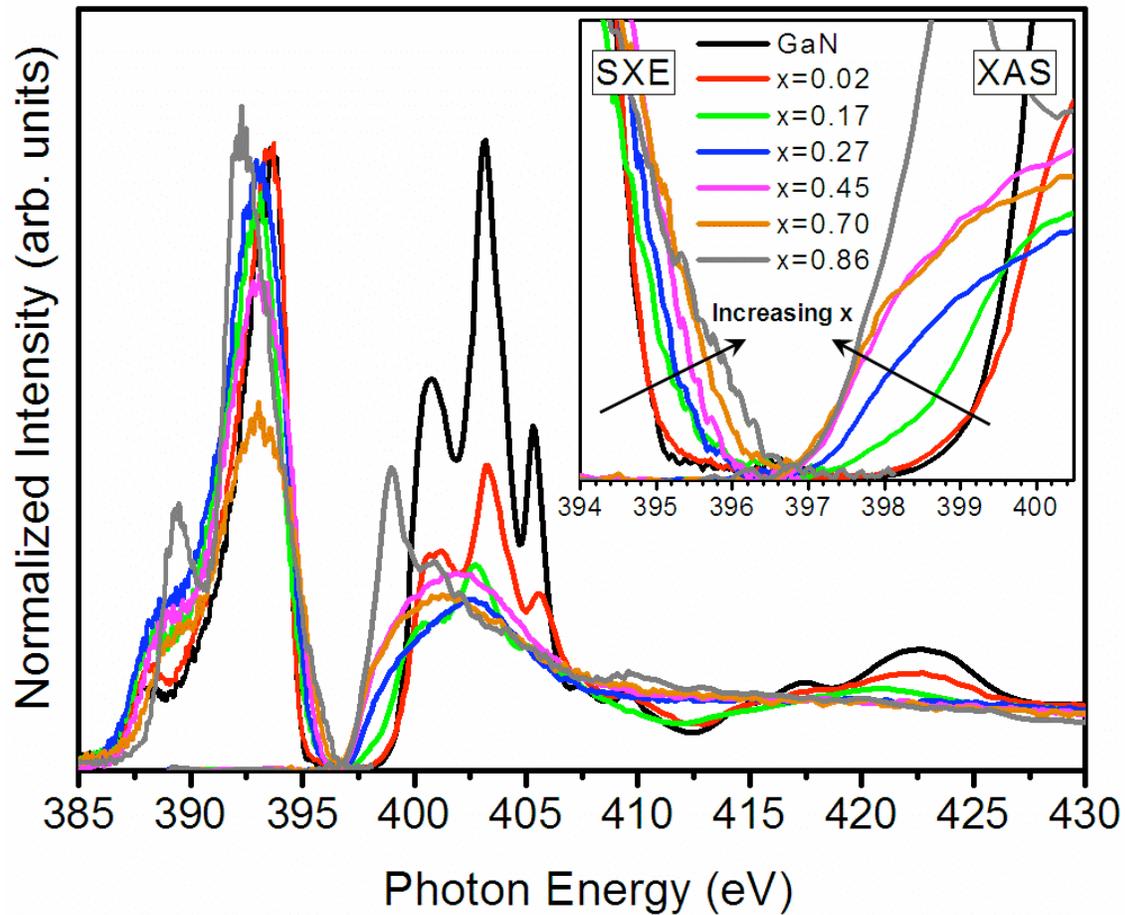
Fig. 7 Fig. 7 The nitrogen *K*-edge SXE and total fluorescence yield XAS of GaN$_{1-x}$As$_x$ films with different As fractions. An elastic emission peak in the threshold-excited SXE is used for energy calibration to XAS. The inset shows the magnified view of the XAS and SXE threshold regions.
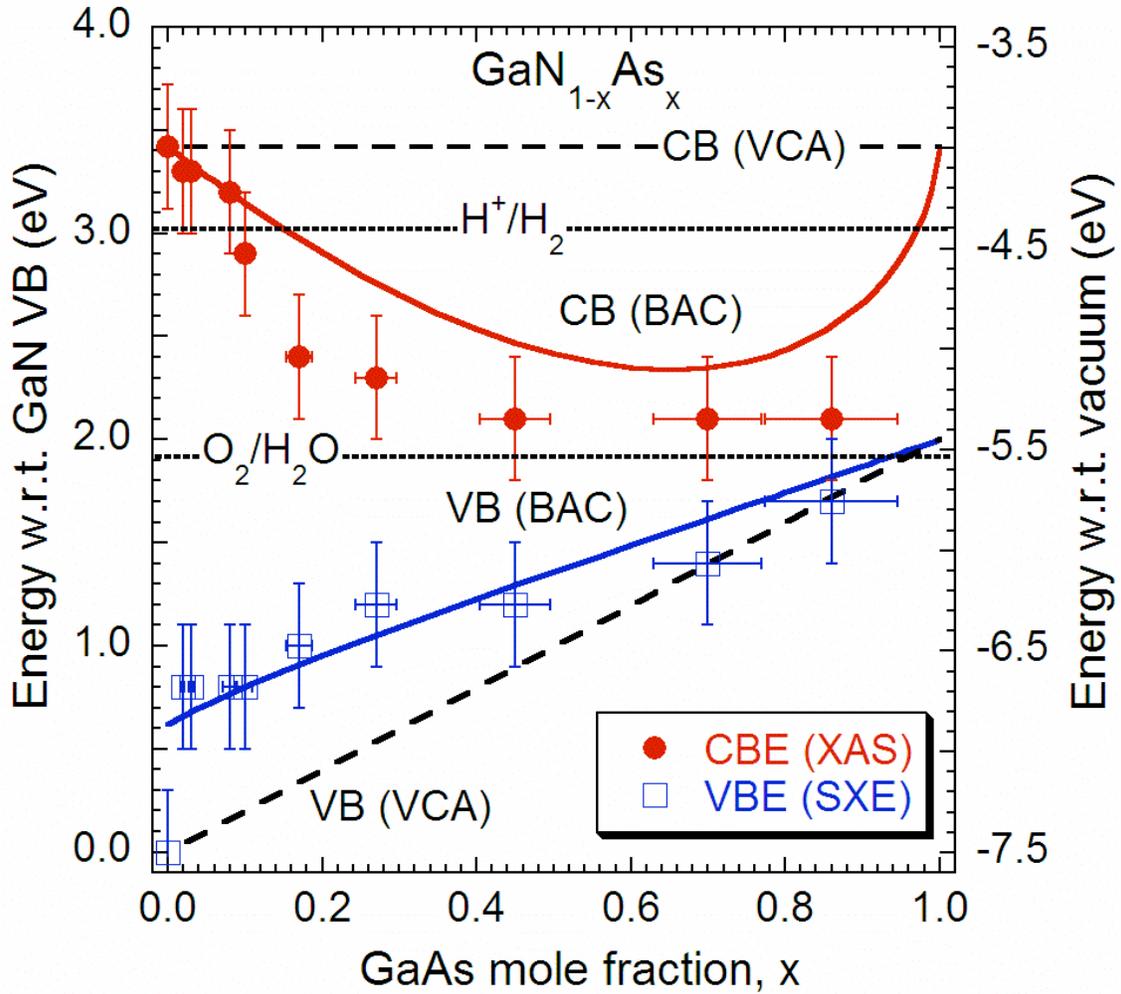
Fig. 8 Composition dependence of the conduction band minimum (CBM) and the valence band maximum (VBM) energies for $GaN_{1-x}As_x$ alloys as measured by XAS and SXE, respectively plotted together with the BAC predicted values. The linear interpolations of CB and VB between end point compounds (GaN and GaAs) are also shown. Positions of the the H_2/O_2 redox potentials with respect to the VB maximum of GaN are also shown.

REFERENCES

[1] W. Shan, W. Walukiewicz, J. W. Ager III, E. E. Haller, J. F. Geisz, D. J. Friedman, J. M. Olson, and S. R. Kurtz, Phys. Rev. Lett. **82**, 1221 (1999).

[2] K. Uesugi, N. Marooka, and I. Suemune, Appl. Phys. Lett., 74, 1254. (1999).

[3] Irina Buyanova and Weimin Chen, eds. Physics and Applications of Dilute Nitrides (Taylor & Francis, New York, 2004).

[4] Ayse Erol ed. Physics of Dilute III-V Nitride Semiconductors and Material Systems: Physics and Technology (Springer-Verlag Berlin-Heidelberg 2008).

[5] M. Kondow, T. Kitatani, S. Nakatsuka, M. C. Larson, K. Nakahara, Y. Yazawa, M. Okai and K Uomi, *IEEE J. Sel. Topics in Quantum Elect.* **3**, 719 (1997).

[6] M. Kondow, T. Kitatani, M. C. Larson, K. Nakahara, K. Uomi and H. Inoue, *J. Crystal Growth* **188**, 255 (1998).

[7] D. J. Friedman, J. F. Geisz, S. R. Kurtz, D. Myers and J. M Olson, *J. Cryst. Growth* **195**, 409 (1998).

[8] S. R. Kurtz, A.A. Allerman, E.D. Jones, J.M. Gee, J.J. Banas, and B.E. Hammons, *Appl. Phys. Lett*. **74**, 729(1999).

[9] C. T. Foxon, I. Harrison, S. V. Novikov, A.J. Winser, R.P. Campion, T. Li, J. of Physics: Condensed Matter 14 (2002) 3383.

[10] A. Kimura, C. A. Paulson, H. F. Tang, and T. F. Kuech, Appl. Phys. Lett. **84**, 1489 (2004).

[11] A. Kimura, H. F. Tang, and T. F. Kuech, J. Cryst. Growth **265**, 71 (2004).

[12] J. Wu, W. Walukiewicz, K. M. Yu, J.D. Denlinger, W. Shan, J.W. Ager, A. Kimura, H.F. Tang, T.F. Kuech, Phys Rev B 70 (2004) 115214.

[13] W.Walukiewicz, W. Shan, K. M. Yu, J. W. Ager III, E. E. Haller, I. Miotlowski, M. J. Seong, H. Alawadhi, and A. K. Ramdas, *Phys. Rev. Lett*. **85**, 1552 (2000).

[14] W. Walukiewicz, K. Alberi, J. Wu, W. Shan, K.M. Yu, and J. W. Ager III, in Physics of Dilute III-V Nitride Semiconductors and Material Systems: Physics and Technology, edited by Ayse Erol (Springer-Verlag Berlin-Heidelberg 2008) Chapter 3.

[15] K. Alberi, J. Wu, W. Walukiewicz, K. M. Yu, O. D. Dubon, S. P. Watkins, C. X. Wang, X. Liu, Y.-J. Cho, and J. Furdyna, Phys. Rev. B **75** (2007) 045203.

[16] K. Alberi, O. D. Dubon, W. Walukiewicz, K. M. Yu, , K. Bertulis and A. Krotkus, Appl. Phys. Lett. **91** (2007) 051909.

[17] K. Alberi, O.D. Dubon, W. Walukiewicz, K.M. Yu, J.A. Gupta, and J.-M. Baribeau, Appl. Phys. Lett. **92**, 162105 (2008).

[18] K. Alberi, J. Blacksberg, L. D. Bell, S. Nikzad, K. M. Yu, O.D. Dubon, W. Walukiewicz, Phys. Rev **B 77**, 073202 (2008).

[19] K. Iwata, H. Asahi, K. Asami, R. Kuroiwa and S. Gonda, Jpn. J. Appl. Phys. **37**, 1436 (1998).

[20] Y. Zhao, F. Deng, S.S. Lau and C.W. Tu, J. Vac. Sci. Technol. **B16,** 1297 (1998).

[21] M. A. Scarpulla, K. M. Yu, O. Monteiro, M. Pillai, M. C. Ridgway, M. J. Aziz, and O. D. Dubon, Appl. Phys. Lett. **82**, 1251 (2003).

[22] K. M.Yu, W. Walukiewicz, J. W. Beeman, M. A. Scarpulla, O. D. Dubon, M. R. Pillai, and M. Aziz, Appl. Phys. Lett. **80**, 3958 (2002).

[23] H. Ohno, *Science* **281**, 951 (1998).

[24] Y. J. Cho, K. M. Yu, X. Liu, W. Walukiewicz, and J. K. Furdyna, Appl. Phys. Lett. **93,** 262505 (2008).

[25] S.V. Novikov, T. Li, A.J. Winser, R.P. Campion, C.R. Staddon, C.S. Davis, I. Harrison and C.T. Foxon, Phys. Stat. Sol. (b) 228 (2001) 223.

[26] P. Stumm and D. A. Drabold, Phys. Rev Lett. 79, 677 (1997).

[27] T. Honda, K. Shimanuki, M. Akiyama, Y. Amahori, H. Kimura, and H. Kawanishi, phys. stat. sol. (c) 0, No. 7, 2678–2681 (2003).

[28] B. J. Ruck, A. Koo, U. D. Lanke, F. Budde, H. J. Trodahl, G. V. M. Williams A. Bittar, J. B. Metson, E. Nodwell, T. Tiedje, A. Zimina and S. Eisebitt, J. Appl. Phys. **96**, 3571 (2004).

[29] Seung Hwan Shim, Kwang Bo Shim,,1, Jong-Won Yoon, Yoshiki Shimizu, Takeshi Sasaki, Naoto Koshizaki, Thin Solid Films **472**, 11 (2005).

[30] S.O. Kucheyev and J.S. Williams, S. J. Pearton, Materials Science and Engineering: R: Reports **33**, 51 (2001).

[31] L. C. Duda, C. B. Stagarescu, J. Downes, K. E. Smith, D. Korakakis, T. D. Moustakas, J. H. Guo, and J. Nordgren, Phys. Rev. B **58**, 1928 (1998).

[32] V. N. Strocov, T. Schmitt, J.-E. Rubensson, P. Blaha, T. Paskova, and P. O. Nilsson, Phys. Rev. **B72**, 085221 (2005).

[33] C. C. Sorrell, S. Sugihara, and J. Nowotny, Eds., *Materials for energy conversion devices* (Woodhead Publishing Limited, Cambridge, England, 2005) ISBN-10:1 85573 932 1.

[34] A.K. Ghosh and H.P. Muruska J Electrochem Soc **124** (1977) 1516.

[35] J. Akikusa and SUM Khan Int J Hydrogen Energy **22** (1997) 875.

[36] O. Khaselev and J. Turner, Science **280** (1998) 425.

[37] J. M. Olson, T. A. Gessert, and M. M. Al-Jasim, *Proceedings 18th IEEE Photovoltaic Specialists Conference*, 552, Las Vegas, Oct. 21–25, 1985 (IEEE, New York, 1985).

[38] K. A. Bertness, S. R. Kurtz, D. J. Friedman, A. E. Kibbler, C. Kramer, and J. M. Olson, Appl. Phys. Lett. **65**, 989 (1994)

[39] A. Luque, A. Marti., Phys. Rev. Lett., **78**, 5014 (1997).